Time-resolved electron spectroscopy for chemical analysis of photodissociation: Photoelectron spectra of $Fe(CO)_5$, $Fe(CO)_4$, and $Fe(CO)_3$

T. Leitner, I. Josefsson, T. Mazza, P. S. Miedema, H. Schröder, M. Beye, K. Kunnus, S. Schreck, S. Düsterer, A. Föhlisch, M. Meyer, M. Odelius, and Ph. Wernet

Citation: J. Chem. Phys. **149**, 044307 (2018); doi: 10.1063/1.5035149
View online: https://doi.org/10.1063/1.5035149
View Table of Contents: http://aip.scitation.org/toc/jcp/149/4
Published by the American Institute of Physics

Time-resolved electron spectroscopy for chemical analysis of photodissociation: Photoelectron spectra of $Fe(CO)_5$, $Fe(CO)_4$, and $Fe(CO)_3$

T. Leitner,[1] I. Josefsson,[2] T. Mazza,[3] P. S. Miedema,[1,a)] H. Schröder,[1,4] M. Beye,[1,a)] K. Kunnus,[1,4,b)] S. Schreck,[1,4,c)] S. Düsterer,[5] A. Föhlisch,[1,4] M. Meyer,[3] M. Odelius,[2,d)] and Ph. Wernet[1,d)]

[1]*Institute for Methods and Instrumentation for Synchrotron Radiation Research, Helmholtz-Zentrum Berlin für Materialien und Energie GmbH, Albert-Einstein-Strasse 15, 12489 Berlin, Germany*
[2]*Department of Physics, AlbaNova University Center, Stockholm University, 106 91 Stockholm, Sweden*
[3]*European XFEL GmbH, Holzkoppel 4, 22869 Schenefeld, Germany*
[4]*Institut für Physik und Astronomie, Universität Potsdam, Karl-Liebknecht-Strasse 24/25, 14476 Potsdam, Germany*
[5]*Deutsches Elektronen-Synchrotron DESY, FS-FLASH, Notkestrasse 85, 22607 Hamburg, Germany*

(Received 13 April 2018; accepted 5 July 2018; published online 27 July 2018)

The prototypical photoinduced dissociation of $Fe(CO)_5$ in the gas phase is used to test time-resolved x-ray photoelectron spectroscopy for studying photochemical reactions. Upon one-photon excitation at 266 nm, $Fe(CO)_5$ successively dissociates to $Fe(CO)_4$ and $Fe(CO)_3$ along a pathway where both fragments retain the singlet multiplicity of $Fe(CO)_5$. The x-ray free-electron laser FLASH is used to probe the reaction intermediates $Fe(CO)_4$ and $Fe(CO)_3$ with time-resolved valence and core-level photoelectron spectroscopy, and experimental results are interpreted with *ab initio* quantum chemical calculations. Changes in the valence photoelectron spectra are shown to reflect changes in the valence-orbital interactions upon Fe–CO dissociation, thereby validating fundamental theoretical concepts in Fe–CO bonding. Chemical shifts of CO 3σ inner-valence and Fe 3p core-level binding energies are shown to correlate with changes in the coordination number of the Fe center. We interpret this with coordination-dependent charge localization and core-hole screening based on calculated changes in electron densities upon core-hole creation in the final ionic states. This extends the established capabilities of steady-state electron spectroscopy for chemical analysis to time-resolved investigations. It could also serve as a benchmark for how charge and spin density changes in molecular dissociation and excited-state dynamics are expressed in valence and core-level photoelectron spectroscopy. *Published by AIP Publishing.* https://doi.org/10.1063/1.5035149

INTRODUCTION

The photodissociation of $Fe(CO)_5$ has always been a prototypical text-book example for understanding how the reactivity in organometallic photoreactions and the dynamics of charge and spin densities are correlated.[1–4] For this understanding, the gas-phase case can be regarded as a reference. Due to the reduced complexity in the gas phase in the absence of solute-solvent interactions, the photodissociation of gas-phase $Fe(CO)_5$ can be regarded a benchmark for new methods to extract charge- and spin-density dynamics from new experimental observables.[5] The loss of multiple CO ligands upon UV photolysis of gas-phase $Fe(CO)_5$ to form $Fe(CO)_4$ and $Fe(CO)_3$ has been established early on.[5–8] Starting the dissociation reactions from a singlet ground state (GS) in $Fe(CO)_5$, the ground states of $Fe(CO)_4$ and $Fe(CO)_3$ in rare-gas matrices were determined experimentally to be triplets.[5,9] The triplet ground state of $Fe(CO)_4$ was confirmed theoretically for the gas phase.[10–12] Based on a combination of earlier evidence[9] with new measured time constants from femtosecond-resolution optical ionization experiments, Fuss and co-workers then proposed a singlet pathway for sequential $Fe(CO)_5$ photodissociation to $Fe(CO)_4$ and $Fe(CO)_3$ [in contrast to synchronous dissociation to $Fe(CO)_4$ and $Fe(CO)_3$ simultaneously].[13] This was summarized by Poliakoff and Turner[14] and is illustrated in Fig. 1(a): After electronic excitation at a wavelength of 266 nm, the dissociation was proposed to proceed from excited singlet-state $Fe(CO)_5$ to excited singlet-state $Fe(CO)_4$ ($^1A_1$) within less than 100 fs with subsequent dissociation of a second CO to $Fe(CO)_3$ with a time constant of 3.3 ps. This singlet pathway was partially confirmed by the detection of singlet-state $Fe(CO)_4$ and its structural characterization in the gas phase with time-resolved electron diffraction by Ihee, Zewail, and co-workers,[15] albeit with a temporal resolution of 10-20 ps and after two-photon excitation with 620 nm.

a)Present address: DESY, FS-FLASH, Notkestrasse 85, 22607 Hamburg, Germany.
b)Present address: PULSE Institute, SLAC National Accelerator Laboratory, Menlo Park, CA 94025, USA.
c)Department of Physics, Stockholm University, AlbaNova University Center, 106 91 Stockholm, Sweden.
d)Authors to whom correspondence should be addressed: wernet@helmholtz-berlin.de and odelius@fysik.su.se

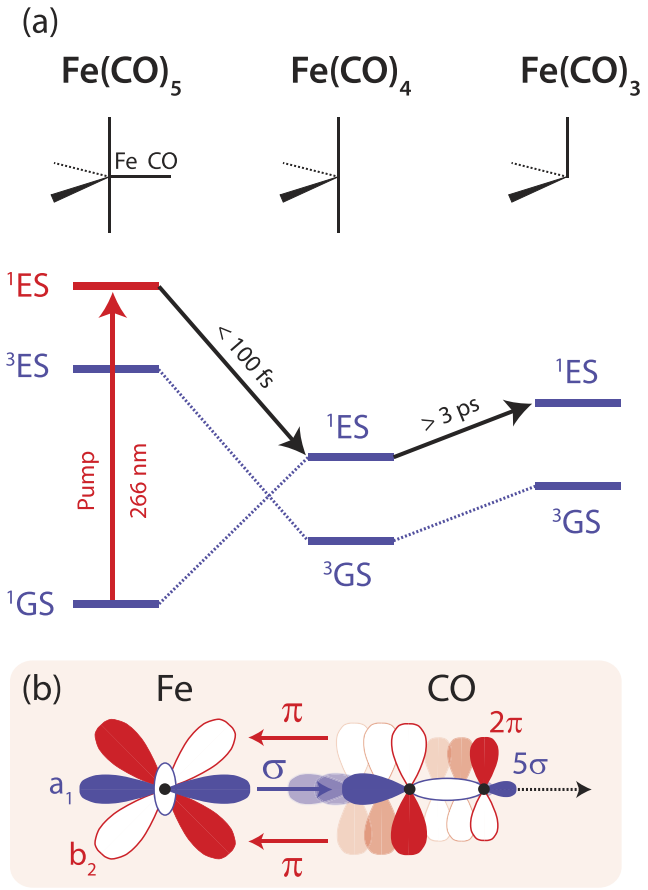

FIG. 1. (a) Molecular structural models depicting the coordination of the Fe center with CO ligands in $Fe(CO)_5$ and illustrating successive CO loss to form the coordinatively unsaturated photofragments $Fe(CO)_4$ and $Fe(CO)_3$ and schematic depiction of the singlet pathway with time constants for gas-phase photodissociation of $Fe(CO)_5$ upon absorption of a photon at 266 nm[13,16] highlighting spin states (singlet and triplet multiplicities) of ground states (GS) and selected excited states (ES) of $Fe(CO)_5$, $Fe(CO)_4$, and $Fe(CO)_3$. (b) Changes in some of the valence electron orbital interactions with Fe-CO dissociation with σ donation (blue, Fe-centered lowest unoccupied molecular orbital, LUMO, interacting with CO highest occupied molecular orbital, HOMO) and π back donation [red, Fe-centered HOMO interacting with CO LUMO, symmetries of Fe-centered orbitals for $Fe(CO)_4$ geometry, different phases depicted with open/closed lobes].

We recently reported an experimental proof for successive dissociation of $Fe(CO)_5$ in the gas phase first to $Fe(CO)_4$ and second to $Fe(CO)_3$ along a singlet pathway with time-resolved optical pump and x-ray probe photoelectron spectroscopy at the x-ray free-electron laser FLASH combined with atomic crystal-field calculations.[16] The detection of free CO molecules based on an unambiguous assignment of the valence photoelectron peaks of uncoordinated CO directly revealed the step-wise occurrence of CO in the dissociation reaction. Multiplet effects in the Fe 3p core-level photoelectron spectra and the reflected intra-atomic Fe core-valence interactions further allowed to determine the singlet spin state of the $Fe(CO)_4$ and $Fe(CO)_3$ photofragments.[16]

Extending this study with a detailed analysis with *ab initio* quantum chemical calculations and additional experimental details, we now report how changes in coordination and charge density or bonding are reflected in the valence and core-level photoelectron spectra of the short-lived reaction intermediates. This study builds on the previously reported kinetic model for sequential dissociation.[13,16] Knowing the relative amounts of all species in the sample as a function of time allows appropriately subtracting the remaining $Fe(CO)_5$ contributions from the measured spectra to extract valence and Fe 3p core-level photoelectron spectra of $Fe(CO)_4$ and $Fe(CO)_3$. The $Fe(CO)_4$ and $Fe(CO)_3$ photoelectron spectra are compared here to the $Fe(CO)_5$ spectra, and the observed chemical shifts are explained with calculated spectra and core-hole induced changes in molecular-orbital interactions, orbital populations, and electron densities. We demonstrate how time-resolved valence and core-level photoelectron spectroscopy[17–24] thereby enable to test fundamental concepts for frontier-orbital interactions and charge-density changes in the dissociation of Fe–CO bonds.[25,26] CO to Fe σ donation and Fe to CO π back donation are reduced upon dissociation, and charge can be thought of as to flow back to the isolated constituents upon deligation, as schematically shown for two of the occupied molecular orbitals in Fig. 1(b) (along the displayed arrows). Here we investigate how these changes in chemical bonding are expressed in the valence and core-level photoelectron spectra. This way of probing valence electronic structure changes upon $Fe(CO)_5$ dissociation in the gas phase complements our earlier investigations of $Fe(CO)_5$ dissociation in solution with time-resolved resonant inelastic x-ray scattering (RIXS).[27,28] Our study contributes to demonstrating how time-resolved photoelectron spectroscopy complements other x-ray based probes of molecular gas-phase dynamics using ion spectroscopy,[29–32] x-ray absorption spectroscopy,[33–37] and x-ray scattering,[38] and it relates to core-hole induced dynamical effects in steady-state x-ray spectroscopy.[30,31,39–42] Our study extends the demonstrated capabilities of time-resolved photoelectron spectroscopy with optical probe pulses,[18,43] and it shows how x-ray photoelectron spectroscopy complements other x-ray methods for the investigation of molecular dynamics.[44–50]

MATERIALS AND METHODS

Experimental set up

The experiment was performed at the x-ray free-electron laser FLASH in Hamburg (Germany)[51,52] with a previously described set up for pump-probe photoelectron spectroscopy,[53] as installed at the PG2 plane grating monochromator beamline[54–56] of the FLASH facility. Some experimental details were partly published previously in Ref. 16, and they are further discussed here. The experimental set up is schematically depicted in Fig. 2. $Fe(CO)_5$ dissociation was initiated with a pump photon at 266 nm, and soft x-ray pulses from FLASH were used to probe the electronic structure and its evolution with time-resolved x-ray photoelectron spectroscopy.

Sample preparation

The $Fe(CO)_5$ and CO samples were prepared in an effusive jet. $Fe(CO)_5$ was purchased from Sigma Aldrich and used without further purification. The liquid sample was evaporated and entered the ultrahigh-vacuum chamber of the set up[53] via

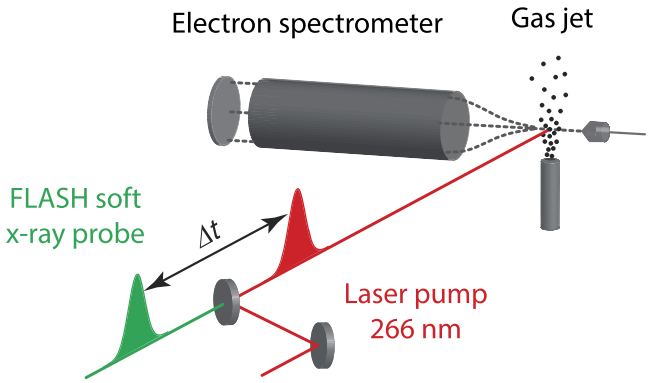

FIG. 2. Schematic of the experimental set up with the effusive gas jet, the magnetic-bottle type electron spectrometer (magnetic tip, drift tube, and detector, with exemplary electron trajectories), and in-coupling of optical laser pump pulses (wavelength 266 nm) collinear with the soft x-ray probe pulses from the FLASH x-ray free-electron laser source (Hamburg, Germany).

a metal tube placed closely below the interaction region. The pressure in the experimental chamber was typically 2-4 10^{-7} mbar during experiments. The sample was kept in the dark and replaced by a fresh sample for each measurement shift to avoid photodecomposition of the sample before reaching the interaction region.

Pump-probe set up

Pump and probe pulses propagated nearly collinearly through the interaction region where pump pulses were coupled into the experimental chamber with a mirror with a central hole on the x-ray propagation axis (Fig. 2). Spatial overlap of pump and probe pulses was established by overlaying the spots of both beams on a Ce:YAG screen in the plane of the gas jet. Temporal overlap was established with an accuracy of ±500 fs from the pump-probe signal at 7.3 eV (Fig. 3) by

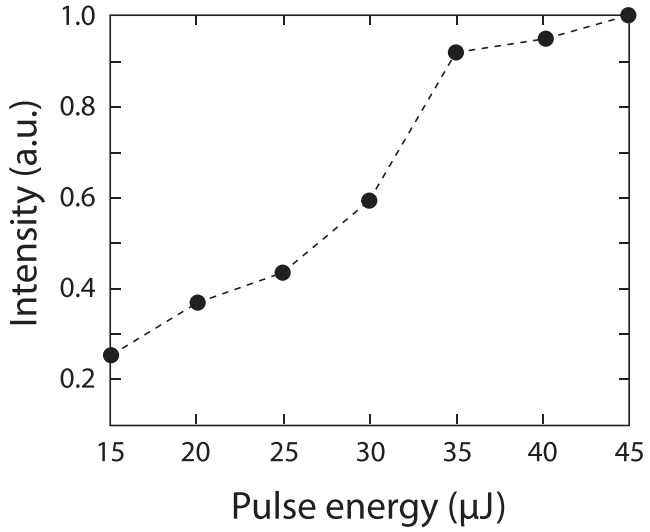

FIG. 3. Variation of the pump-probe effect [photoelectron intensity of the peak at 7.3 eV in the transient difference spectra in Fig. 1(b) of Ref. 16; see also the difference spectrum in Fig. 5(a)] with pump-laser pulse energy (normalized to one at maximum). Throughout this study, a pump-pulse energy of 25 μJ/pulse was used (pump fluence 7 mJ/cm^2, pump peak intensity 1.2×10^{11} W/cm^2).

comparing the photoelectron spectra for a series of nested delay time intervals on a LeCroy digital oscilloscope stepwise. The overall temporal resolution was measured with the photoelectron spectra to be 1.0 ± 0.3 ps (Gaussian FWHM). The temporal resolution was limited by (i) the temporal jitter between electron bunch and optical laser (~500 fs FWHM[57] at the time of data acquisition), (ii) slow drifts of the effective relative arrival time of pump and probe pulses on a minute scale, and (iii) the x-ray pulse stretching by the PG2 beamline monochromator grating. With the employed spot size (see below), the pointing jitter of pump and probe beams was negligible.

Optical pump beam parameters and $Fe(CO)_5$ excitation yield

The optical laser used for photo-excitation of the sample had a wavelength of 266 nm obtained by third-harmonic generation of a Ti:Sa laser of the FLASH facility with a pulse duration of the 266 nm pulses of 150 fs at a repetition rate of 10 Hz (2 mJ/pulse and pulse durations of 60 fs for the 800 nm fundamental).[58] The employed pulse energy was 25 μJ/pulse [third-harmonic generation with two BBO frequency conversion crystals in sequential arrangement with UV dielectric mirrors to separate fundamental and second harmonics]. The intensity of the pump-probe signal (one of the transient valence photoelectron signals) is plotted as a function of the pump-pulse energy in Fig. 3. It saturates at a pump-pulse energy of around 35 μJ/pulse, and we thus chose to pump with 25 μJ/pulse to stay in a regime with non-saturated signals. We found no indication of multiphotons nor any other non-linear effects by the pump laser. The spot size of the 266 nm radiation as measured on the Ce:YAG screen in the interaction region was 500 μm in the horizontal and 700 μm in the vertical (FWHM values as determined with a two-dimensional Gauss fit of the imaged spot), thus well over-illuminating the x-ray probe beam spot. With the corresponding pump fluence of 7 mJ/cm^2 (pump peak intensity 1.2×10^{11} W/cm^2), a fraction of 6.2 ± 0.4% of the sample was excited (the employed pump intensity is higher than the 10^9 W/cm^2 used in Ref. 13 and lower than the 10^{14} W/cm^2 used in Ref. 6 or the 10^{13} W/cm^2 for 2-photon excitation with 620 nm in Ref. 15). The kinetic model developed in Ref. 16 is reproduced in Fig. 4(a). The detected $Fe(CO)_5$ content and its depletion are shown as a function of pump-probe delay time in Fig. 4(b).

FLASH x-ray probe beam parameters

The mean photon energy was set to 123 eV with an free-electron laser (FEL) bandwidth of about 1% and the repetition rate of the experiment was 10 Hz. The x-ray pulse energies before the monochromator amounted to 20-40 μJ/pulse as measured with a gas monitor detector provided by the FLASH facility.[59] The x-ray pulse duration before the monochromator was approximately 100 fs (FWHM), as determined by electron-bunch length measurements.[60] The PG2 beamline is a grating monochromator beamline where we used a 200 l/mm grating.[54–56] The exit slit was set to a size of 200 μm and the c_{ff} value used was 1.5. This resulted in a bandwidth of 0.1 eV

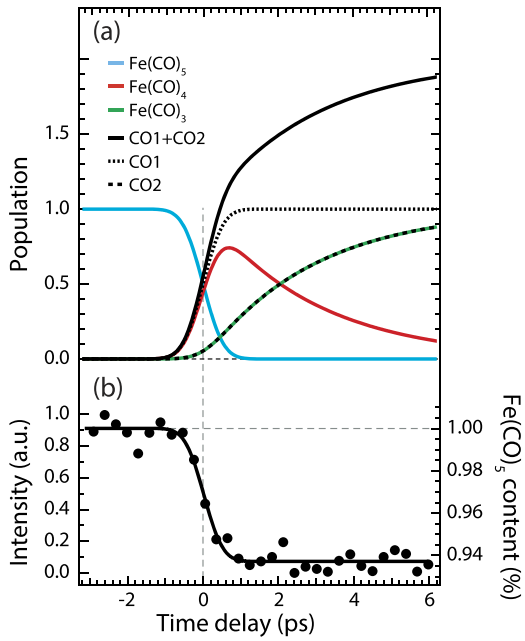

FIG. 4. (a) Components of the kinetic model developed in Ref. 16 representing populations of corresponding species for sequential $Fe(CO)_5$ photodissociation first to $Fe(CO)_4$ and CO (termed as CO1 here) and second to $Fe(CO)_3$ and CO (termed as CO2 here). (b) Measured integrated intensities versus pump-probe delay time representing $Fe(CO)_5$ depletion [closed circles, integrated for binding-energy region 9.7-10.0 eV in the transient difference spectra in Fig. 1(a) in Ref. 16; see also the difference spectrum in Fig. 5(a)] with the best fit of the kinetic model for $Fe(CO)_5$ depletion and corresponding to the $Fe(CO)_5$ content in the sample (solid line, intensities normalized to one at maximum). Other measured integrated intensities used to fit the kinetic model for binding-energy regions representing $Fe(CO)_4$, $Fe(CO)_3$, CO1, and CO2 can be found in Ref. 16.

(FWHM). The x-ray pulse energies at the sample (after the monochromator) were estimated to be 0.1-1 μJ corresponding to 10^{10}-10^{11} photons/s (at 10 Hz and in an 0.1% bandwidth). The x-ray spot size was measured in the interaction region by imaging the spot on a Ce:YAG screen installed in the experimental vacuum chamber in the plane of the gas jet. The x-ray spot had an elliptical shape with a measured size of 280 μm in the horizontal and 400 μm in the vertical for the respective FWHM values, as determined with a two-dimensional Gauss fit of the imaged spot.

Photoelectron spectroscopy

Photoelectrons were detected at an angle of 90° with respect to the propagation axes of pump and probe beams (Fig. 2). Photoelectron kinetic energies were analyzed with a magnetic-bottle-type time-of-flight electron spectrometer where electrons were amplified and detected by a multichannel-plate stack operated in the current mode.[53] A retardation voltage of 95 V was used for valence photoelectron spectroscopy and 30 V was used for core-level photoelectron spectroscopy to suppress contributions from slow electrons to the spectrum. The electron-energy bandwidth of the spectrometer amounts to 5% of the pass energy (of the retarded kinetic energy). For the kinetic energies of 118-103 eV in valence photoelectron spectroscopy, the pass energies were thus 23-8 eV and the bandwidth resulted in 0.4-1.2 eV (Gaussian FWHM). For the kinetic energy of 60 eV (88 eV) in Fe 3p core-level (CO 3σ inner-valence) photoelectron spectroscopy, the pass energies was thus 30 eV (60 eV) and the bandwidth resulted in 1.5 eV (3 eV, Gaussian FWHM).

Data acquisition and analysis

The electron yield was stored via a digital oscilloscope or directly to the FLASH data storage system via a network connected 10 bit *Acqiris* digitizer system provided by FLASH. For enabling sorting of the data with respect to pump-probe delay times, photoelectron energy distributions were measured separately for each shot. Shots with very few or no x-ray photons were discarded from the analysis. Correction of the pump-probe delay time (minute/hour drifts of the effective relative arrival time of pump and probe pulses) was done by sorting the measured data according to the correlation of optical laser pulses and dipole radiation from the FLASH electron bunches as measured with a streak camera.[58] As the streak camera gave an averaged signal, a shot-to-shot correction of the pump-probe delay time was not available at the time of the experiment. The time-delay bin size was 50 fs in the raw data and they were re-binned to 300 fs for valence photoelectron spectra and to 250 fs for core-level photoelectron spectra in the displayed data. Accumulation times amounted to 3.9 h for the reported valence photoelectron spectra (~150 000 shots) and 4.7 h for the reported core-level photoelectron spectra (~170 000 shots). The binding-energy axis was calibrated with well-known binding energies of rare-gas samples and cross-checked with published binding energies for spectra of $Fe(CO)_5$. Intensity of the spectra was normalized for each time-delay bin to the same spectral area, hence to the same total number of electron counts per spectrum (normalization to the incident photon flux I_0 was not possible because a signal proportional to I_0 after the monochromator exit slit could not be measured).

Multiconfigurational self-consistent-field calculations of geometries and binding energies

Geometry optimization and photoelectron binding energy calculations were performed within multiconfigurational self-consistent field (MCSCF) theory, using the MOLCAS 8.0 software.[61] The geometries of the $Fe(CO)_5$ complex and its photoproducts $Fe(CO)_4$ and $Fe(CO)_3$ were optimized at the complete active space perturbation theory CASPT2(12, 12) level of theory[62] using a basis set of triple-zeta valence with polarization quality (ANO-RCC-VTZP).[63,64] In this quantum chemical treatment, electronic relaxation in the final states is accurately treated similar to the calculations of Grell *et al.*[65] The photoelectron binding energies including spin-orbit coupling were computed as energy differences between the CASPT2(10, 10) (for the valence spectra) and restricted active space SCF (RASSCF)(3, 10, 0; 16, 1, 0) (for the core-level spectra) neutral initial and cationic final states.[61] Specifically, the vertical transition energies from the initial ground state of the gas-phase geometry to an electronically relaxed final ionized state, including relativistic effects, but neglecting the zero point energy, were calculated. The active space for constructing the restricted active space SCF

(RASSCF)[66] wavefunction of the initial state and the final ionized states comprised 10—9 for the ion—electrons in 10 valence orbitals, including Fe 3d. All possible permutations of the 10 electrons (9 for the valence ionized states) over these orbitals were permitted in the calculations. Since the set of orbitals does not involve Fe 3p, the active space in the calculations of the Fe 3p photoelectron spectra also contained these three orbitals, limited to have at most one hole in order to allow for photoionization. The active spaces of the initial and final, ionized, states are denoted as RASSCF(16, 1, 0; 3, 10, 0) and RASSCF(15, 1, 0; 3, 10, 0), respectively. To ensure convergence in the RASSCF, the Fe 3p orbitals were kept fixed at their shape from a preceding Hartree-Fock calculation of the initial ground state. As there were no restrictions on the orbital occupation within the active space of the Fe 3d spectrum calculations, the initial and final (valence ionized) wavefunctions were equivalent to complete active space SCF [CASSCF(10, 10)/CASSCF(9, 10)] wavefunctions.[67] The calculated Fe 3d binding energies included dynamic electron correlation effects through a second order perturbative treatment of the multiconfigurational wavefunctions (CASPT2). Relativistic effects were taken into account in two steps, using the scheme implemented in MOLCAS. First, based on configuration state functions of specific multiplicities, the set of multiconfigurational states were calculated in a spin-free approach, with the scalar terms of the second order Douglas–Kroll transformation of the relativistic Hamiltonian.[68,69] Through state averaging, the orbitals of each ion were optimized for the energy average of the lowest final states, giving rise to the main spectral lines. They are natural orbitals derived from the state-averaged density matrix, and below we discuss their natural occupation numbers. In the second step, the spin-orbit coupling matrix elements were computed using the RASSCF/CASPT2 energies of these 3/4 states as the interaction between wavefunctions of pure multiplicities.[70] In order to give accurate results, all strongly coupled states must be included, and the active space must be sufficiently flexible to describe them well. Transition intensities of the different fine-structure components could not be calculated and were arbitrarily set to the same values.

Calculations of convoluted line spectra

From the calculations, we obtain for each initial state a set of transitions (stick spectrum) representing the discrete set of ionization channels. For the calculated valence photoelectron spectra, each transition (stick) was replaced by a Gaussian profile of corresponding binding energy and intensity with a FWHM of 1.1 eV reflecting the experimental bandwidth (combined photon-energy and electron-kinetic-energy bandwidths). For the calculated Fe 3p core-level photoelectron spectra, each stick was replaced by a Lorentzian profile of corresponding binding energy and intensity with a FWHM of 1.2 eV to account for lifetime broadening.[71] The resulting sum of Lorentzians was convoluted with the experimental bandwidth of 1.5 eV (FWHM, the Gaussian profile resulting from the combined photon energy and electron kinetic energy bandwidths).

Calculations of charge densities and orbital populations upon Fe 3p core-hole creation

The changes in the electronic structure (charge densities) upon ionization of the Fe 3p core orbitals were rationalized in terms of electron density differences between the average density of the three final ionic states and the density of the ground state. This was complemented with calculated differences in the orbital occupation numbers obtained for the final and initial RASSCF wavefunctions.

RESULTS AND DISCUSSION

The measured time-resolved valence photoelectron spectra following photoexcitation of $Fe(CO)_5$ in the gas phase at 266 nm with dissociation to $Fe(CO)_4$ within less than 100 fs and subsequent dissociation of $Fe(CO)_4$ to $Fe(CO)_3$ with a time constant of 3.3 ps are shown in Fig. 5(a). The spectra are dominated by peaks due to photoionization from the Fe 3d orbitals at 8 and 9.5 eV and CO σ and π orbitals at 14.5 and 18 eV in

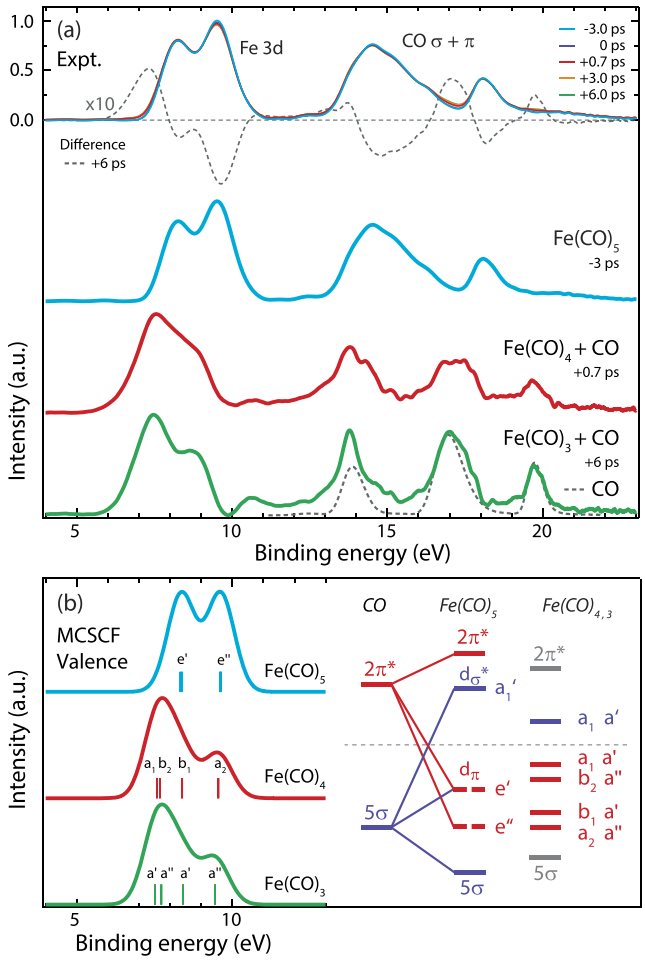

FIG. 5. (a) Measured valence photoelectron spectra at indicated pump-probe delay times (dashed line: transient difference spectrum at +6 ps, multiplied by 10) with dominant contributions (from top to bottom) of $Fe(CO)_5$, $Fe(CO)_4$, and $Fe(CO)_3$ (dashed line: separately measured spectrum of free CO). (b) Multi-configurational self-consistent-field (MCSCF) calculations of valence photoelectron spectra of $Fe(CO)_5$, $Fe(CO)_4$, and $Fe(CO)_3$ (all in the singlet state) and of a molecular-orbital diagram [π interactions: red, σ interactions: blue, orbital symmetries e′, e″ for geometries of $Fe(CO)_5$, a_1, b_2, b_1, a_2 for $Fe(CO)_4$, a′, a″ for $Fe(CO)_3$].

$Fe(CO)_5$.[16,72–74] Depletion of these $Fe(CO)_5$ signals is visible for increasing pump-probe time delay as well as new intensities due to $Fe(CO)_4$, $Fe(CO)_3$, and free CO arising at 7 and 17 eV [emphasized by the 6 ps transient difference spectrum in Fig. 5(a)]. The kinetic model in Fig. 4(a) as established in our earlier study[16] can now be used to determine the pump-probe delay times with maximal $Fe(CO)_4$ and $Fe(CO)_3$ contributions. According to this kinetic model, the $Fe(CO)_4$ and $Fe(CO)_3$ contributions are maximal at 0.7 ps and 6 ps, respectively. The fitted $Fe(CO)_4$:$Fe(CO)_3$ ratios amount to 0.74:0.21 at 0.7 ps [with a remaining fraction of 0.05 of $Fe(CO)_5$ which, in the fit shown in Fig. 4(a), corresponds to the optically excited $Fe(CO)_5$ molecules only] and 0.13:0.87 at 6 ps. The kinetic model further allows us to determine the $Fe(CO)_5$ content in the sample, including the non-excited $Fe(CO)_5$ molecules, as a function of pump-probe delay time as shown in Fig. 4(b). We determine the $Fe(CO)_5$ contents at 0.7 ps and 6 ps to 0.940 and 0.935, respectively. Subtracting the $Fe(CO)_5$ spectrum scaled by these amounts from the spectra at 0.7 ps and 6 ps in Fig. 5(a) resulted in the valence photoelectron spectra dominantly representing $Fe(CO)_4$, $Fe(CO)_3$, and free CO, also shown in Fig. 5(a). At binding energies above 13 eV, signals of free CO dominate the underlying signals of CO bound in $Fe(CO)_4$ and $Fe(CO)_3$. With the aim of characterizing bonding in the short-lived reaction intermediates $Fe(CO)_4$ and $Fe(CO)_3$ by a detailed analysis of the photoelectron spectral shapes, we therefore concentrate on the Fe 3d peaks in $Fe(CO)_4$ and $Fe(CO)_3$ as compared to $Fe(CO)_5$ at around 8 eV [our current signal to noise ratio precludes subtracting the free CO signals of the spectra in Fig. 5(a) in addition to subtracting the $Fe(CO)_5$ contributions].

The shift of the Fe 3d peaks by −0.7 eV when going from $Fe(CO)_5$ to $Fe(CO)_4$ and the redistribution of intensity from the high to the low binding-energy multiplet peak as well as the negligible changes between $Fe(CO)_4$ and $Fe(CO)_3$ are reproduced by our calculated spectra based on the multi-configurational quantum chemical approach in Fig. 5(b). We assign here the calculated ionic final-state energies in the spectra to ionizations from the respective molecular orbitals according to the calculated molecular-orbital diagrams shown in Fig. 5(b). This cannot be expected to result in a one-to-one correspondence of peak binding energies and orbital energies, but it approximately links the spectral changes to changes in the frontier-orbital interactions upon deligation. Under the mean-field approximation, Koopmans' theorem states that electron binding energies can be represented by Hartree-Fock orbital energies. However, different ionic final states experience different electron relaxation, and accurate calculations require explicit calculations of each final state. In many systems, high-level multi-configurational calculations are required for trustworthy simulations of photoelectron spectra. Notice that in Fig. 5(b) we compare the experimental data to calculated binding energies including explicit treatment of the initial and final states in the ionization process, whereas in Fig. 5(c), we depict the orbital level diagram. The validity of this approach was demonstrated for the valence photoelectron spectrum of $Fe(CO)_5$,[72,73] it has been used in the interpretation of x-ray spectroscopic results of CO bound to Fe,[75] and is used here for interpretation of the $Fe(CO)_4$ and $Fe(CO)_3$ spectra (we discard the LUMO as only occupied orbitals are probed with photoelectron spectroscopy). We also note that there are small differences between our calculated MO diagram and the one reported in Ref. 26. We believe that this is due to the differences in the computational methods used.

The step-wise detachment of carbonyl groups results in changes in point group symmetry from D_{3h} in $Fe(CO)_5$ to C_{2v} in $Fe(CO)_4$ and subsequently C_s in $Fe(CO)_3$, and we use the corresponding irreducible representations in Fig. 5(b) to denote the orbitals. It is known that removing CO from $Fe(CO)_5$ splits e″ into a_2 and b_1 and e′ into b_2 and a_1 in $Fe(CO)_4$, and a_2 is the only orbital not involved in bonding as it overlaps only weakly with the ligand orbitals.[26] Our calculations [Fig. 5(b)] show that the a_2 peak in $Fe(CO)_4$ retains the energy of the e″ peaks in $Fe(CO)_5$ thereby confirming that the a_2 orbital is not involved in bonding. All other orbitals (a_1, b_2, and b_1) are involved in Fe–CO bonding and are hence delocalized to some extent over all ligands.[26] Removing one ligand reduces the interactions of the a_1, b_2, and b_1 orbitals with ligand orbitals. In Fig. 1(b), this reduction of orbital interactions upon ligand dissociation is depicted for the π-back-donation interactions of the b_2 orbital. With a simple picture in mind where reducing covalent interactions increases the energies of occupied orbitals, the increase of orbital energies of a_1, b_2, and b_1 [Fig. 5(b)] can be thereby intuitively understood. This assessment is validated by our calculations as the calculated binding energies of the corresponding photoelectron peaks decrease. The reduction of covalent interactions thus explains the experimentally observed shift of the Fe 3d peaks to lower binding energies when going from $Fe(CO)_5$ to $Fe(CO)_4$. Likewise, the calculated redistribution of energies of the respective Fe 3d fine-structure components also explains the redistribution of the spectral weight from higher to lower binding energies in the Fe 3d peaks in the experiment. The orbital-energy changes from $Fe(CO)_4$ to $Fe(CO)_3$ are known to be much smaller than the changes from $Fe(CO)_5$ to $Fe(CO)_4$[1,73] explaining corresponding negligible spectral differences in both experiment and theory between $Fe(CO)_4$ and $Fe(CO)_3$. Our data thus validate fundamental theoretical concepts of how valence molecular-orbital interactions change upon Fe–CO deligation.[25,26]

Having established how the changes in coordination and charge density or bonding are reflected in the valence photoelectron spectra, we now turn to the inner-valence and element- and site-specific core-level photoelectron spectra. The aim is to analyze in detail the chemical shifts of the spectra in the spirit of the original publications on electron spectroscopy for chemical analysis (ESCA).[76–78]

The measured time-resolved inner-valence and core-level photoelectron spectra and their differences are shown in Figs. 6(a) and 6(b) for selected delays. Based on seminal photoelectron spectroscopy and investigations of $Cr(CO)_6$ and of CO deposited on surfaces,[79–82] the broad peak around 36 eV can be straightforwardly assigned to electron emission from the inner-valence 3σ orbital of CO bound in $Fe(CO)_5$ where the 3σ orbital is derived from the atomic 2s orbitals of C and O. The peak at 63 eV was determined before to arise from the emission from the Fe 3p core level in $Fe(CO)_5$,[83] and we

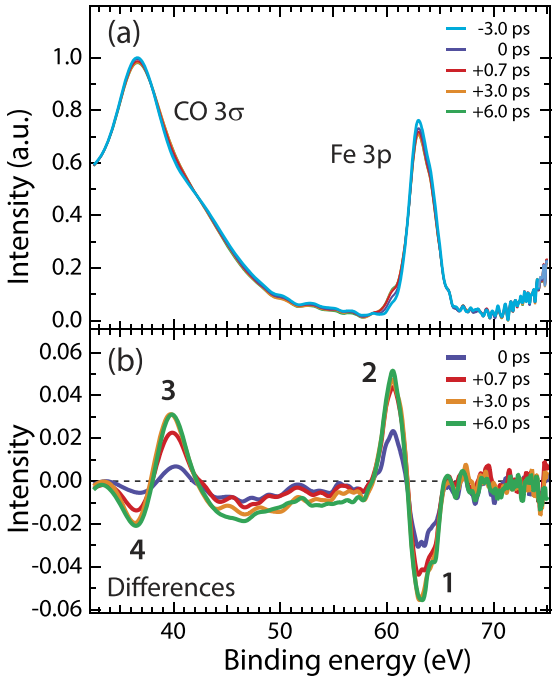

FIG. 6. (a) Fe 3p core-level and CO 3σ inner-valence spectra of $Fe(CO)_5$ measured at a photon energy of 123 eV and the given delay times after optical excitation at 266 nm. (b) Difference spectra at indicated delay times (positive delays are pumped before probe pulses; for each difference spectrum, the spectrum corresponding to unpumped molecules at −3 ps was subtracted from the measured intensities). Intensities at −3.0 ps normalized to one at maximum; numbers 1-4 are binding-energy regions for which the temporal evolution of intensities is plotted in Fig. 7. Data in the Fe 3p binding-energy region were previously published in Ref. 16.

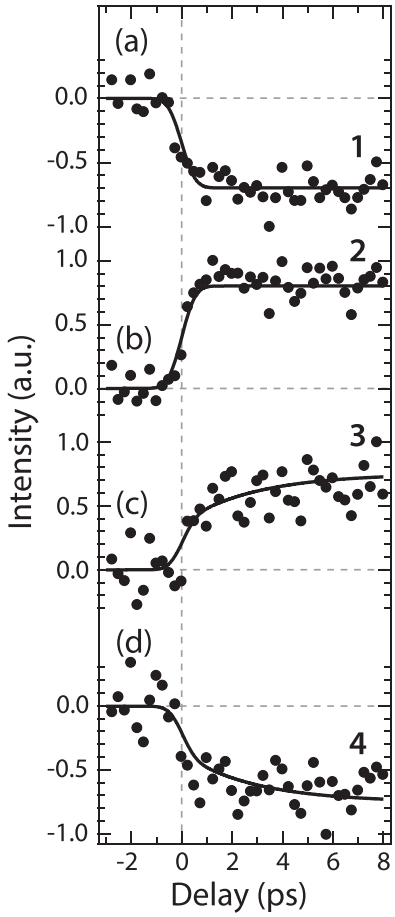

FIG. 7. [(a)–(d)] Measured integrated intensities versus pump-probe delay time (closed circles) with the kinetic model (solid lines) taken from Fig. 4 without adjustments of parameters (except for relative intensities). Intensities (normalized to one/minus one at maximum/minimum) were integrated for binding-energy regions (a) 62-65.5 eV (peak 1 in Fig. 6), (b) 58.5-62 eV (peak 2 in Fig. 6), (c) 38-42 eV (peak 3 in Fig. 6), and (d) 35-38 eV (peak 4 in Fig. 6). Solid lines in (a)–(d) are (a) depletion of $Fe(CO)_5$, (b) sum of $Fe(CO)_4$ and $Fe(CO)_3$, (c) sum of CO1 and CO2, and (d) depletion of CO bound in $Fe(CO)_5$ and $Fe(CO)_4$. Data in (b) (up to 6 ps) were previously published in Ref. 16.

analyzed its shape in our previous study for determining the spin states of $Fe(CO)_5$ and $Fe(CO)_4$ at 0.7 ps and $Fe(CO)_3$ at 6 ps to singlet.[16] The region in between 43 and 58 eV is dominated by so-called shake-up satellites[79,82] and it is not further analyzed here. The temporal evolutions of the binding-energy regions 1-4 [Fig. 6(b)] are plotted in Figs. 7(a)–7(d) and they are found to agree well with the kinetic model also plotted in Fig. 7. Due to the limited signal to noise ratio of our data in Fig. 7, we do not claim this agreement to represent an independent confirmation of the kinetic model. We merely use the agreement to assign regions 1-4 to the corresponding species: $Fe(CO)_5$ depletion in region 1, sum of $Fe(CO)_4$ and $Fe(CO)_3$ in region 2, rise of free CO in region 3, and depletion of CO bound in $Fe(CO)_5$ and $Fe(CO)_4$ in region 4 (equaling the negative of the rise of free CO). Following our procedure for the valence photoelectron spectra and based on the determined amount of $Fe(CO)_5$ as a function of pump-probe delay time, the photoelectron spectra with dominant fractions of $Fe(CO)_4$, $Fe(CO)_3$, and free CO were determined by subtracting appropriately scaled $Fe(CO)_5$ spectra from the spectra shown in Fig. 6(a) at 0.7 and 6 ps. The resulting CO 3σ inner-valence and Fe 3p core-level photoelectron spectra of $Fe(CO)_5$ and $Fe(CO)_4$ plus free CO and $Fe(CO)_3$ plus free CO are displayed in Fig. 8 (data were integrated over ±0.2 ps around the given delays). Illustrating the established notion of site-specificity of core-level photoelectron spectroscopy, these spectra reflect the different chemical shifts of the Fe 3p peak in $Fe(CO)_5$, $Fe(CO)_4$, and $Fe(CO)_3$ and of the 3σ peak of CO bound in $Fe(CO)_5$, $Fe(CO)_4$, and $Fe(CO)_3$ and of free CO. The CO 3σ peak shifts by +2.8 eV (to higher binding energies) when going from CO bound in $Fe(CO)_5$ to free CO. This transient shift is comparable (in sign and direction) to the steady-state shift of +2.5 eV measured for CO bound in $Cr(CO)_6$ relative to free CO.[79,82] Furthermore, and with less certainty due to missing calculations, the 3σ peak of CO bound in $Fe(CO)_4$ is found to shift by −2 to −3 eV relative to $Fe(CO)_5$ with a negligible shift in $Fe(CO)_3$ compared to $Fe(CO)_4$ (see the shoulders around 34 eV in the 0.7 and 6 ps spectra in Fig. 8, albeit poorly resolved due to a larger bandwidth in this binding energy region; see the section named materials and methods). The Fe 3p peak shifts by −2.2 eV (to lower binding energies) when going from $Fe(CO)_5$ to $Fe(CO)_4$ and does not further change for $Fe(CO)_3$ compared to $Fe(CO)_4$. Dissociation of $Fe(CO)_5$ thus creates a number of different classes of chemically different environments for Fe and CO and our data demonstrate how their evolution in time can be selectively probed with time-resolved core-level photoelectron spectroscopy via their different chemical shifts.

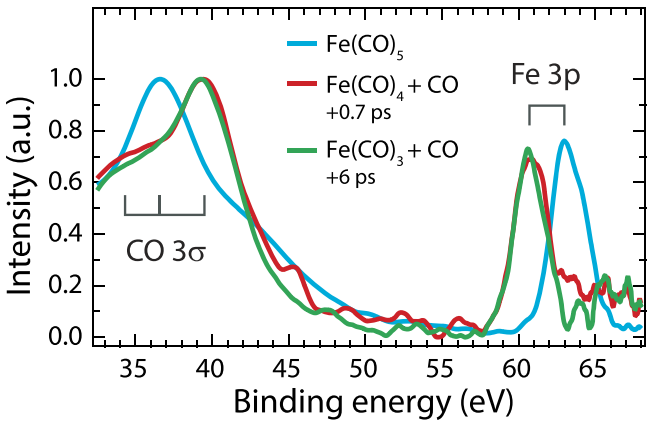

FIG. 8. Fe 3p core-level and CO 3σ inner-valence photoelectron spectra of $Fe(CO)_5$, $Fe(CO)_4$, $Fe(CO)_3$, and free CO where bar diagrams indicate the different binding energies (chemical shifts) of the different chemical sites of (in the order of decreasing energy) the Fe 3p peak of $Fe(CO)_5$, Fe 3p peak of $Fe(CO)_4$ and $Fe(CO)_3$, CO 3σ peak of free CO, CO 3σ peak of CO in $Fe(CO)_5$, and CO 3σ peak of CO in $Fe(CO)_4$ and $Fe(CO)_3$ (intensities normalized to one at maximum).

We now turn to a detailed analysis of the Fe 3p binding energy which decreases from $Fe(CO)_5$ to $Fe(CO)_4$ and therefore seems to correlate with the coordination of the Fe center. For this, we first remind that the valence photoelectron spectra were analyzed based on changes in neutral ground-state molecular-orbital energies (no ionization included), and these changes were found to correlate with shifts of corresponding ionic final-state photoelectron peaks. The question arises about how to relate the changes in the one-electron molecular-orbital interactions to the Fe 3p binding energy shifts. The fact that the Fe 3p peak does not shift further when going from $Fe(CO)_4$ to $Fe(CO)_3$ shows that there is no linear relationship between the Fe 3p chemical shift and coordination.

We use calculated spectra to analyze this finding, and the Fe 3p photoelectron spectra of singlet-state $Fe(CO)_5$, $Fe(CO)_4$, and $Fe(CO)_3$ as calculated with our MCSCF approach are displayed in Fig. 9. The spectra qualitatively reproduce the experimentally observed shift to lower binding energies when going from $Fe(CO)_5$ to $Fe(CO)_4$ and the negligible shift when comparing $Fe(CO)_4$ and $Fe(CO)_3$. The shift, however, is underestimated by about 50% compared to the experiment probably due to the neglect of core-orbital relaxation upon structural changes. In turn, this approximation of not allowing the structure and core orbitals to relax upon 3p ionization enables quantifying the effect of core-hole creation on the electronic structure of the system. Following the established notions of steady-state core-level photoelectron spectroscopy,[76–78] this therefore allows us to explain the Fe 3p chemical shift with core-hole effects in the ionic final states of the systems.[84,85] This represents our first and well-controlled step toward understanding the Fe 3p shift, and forthcoming analyses will have to show how important effects due to structural and core-orbital relaxation are.

To quantify core-hole effects on the electronic structure and following classical approaches to quantify core-hole effects,[79,81] we evaluate the calculated electron-density differences (differences between the electronic structures with and without the Fe 3p core hole) for $Fe(CO)_5$, $Fe(CO)_4$, and

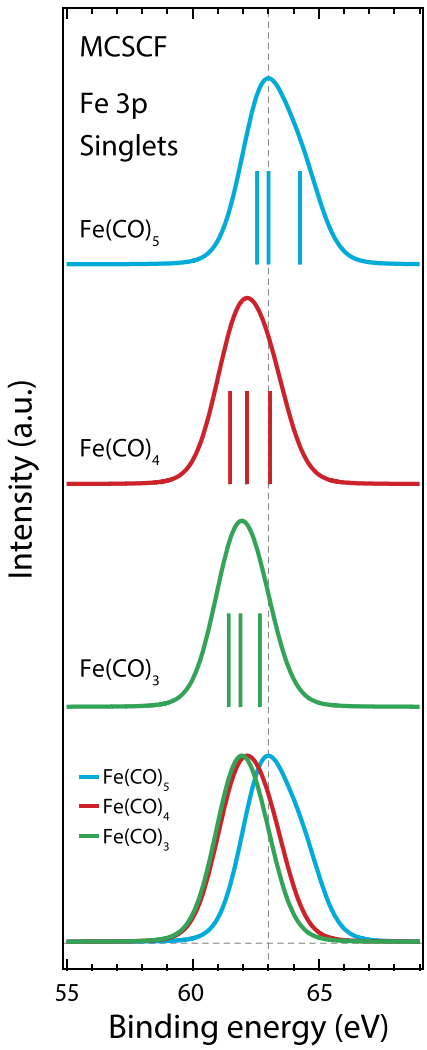

FIG. 9. Multiconfigurational self-consistent-field (MCSCF) calculations of Fe 3p photoelectron spectra for singlet-state $Fe(CO)_5$, $Fe(CO)_4$, and $Fe(CO)_3$ [sticks are calculated binding energies of the final ionic states, $Fe(CO)_5$ spectrum shifted to match the experiment with 63 eV at maximum, $Fe(CO)_4$ and $Fe(CO)_3$ spectra shifted by the same amount, and intensities of all spectra normalized at maximum].

$Fe(CO)_3$ in Fig. 10. We find in our calculations that Fe 3p core-hole creation causes electron-density changes throughout the molecule. $Fe(CO)_5$ serves as a reference, and additional changes in $Fe(CO)_4$ or $Fe(CO)_3$ explain the calculated chemical shifts with respect to $Fe(CO)_5$. Fe 3p core-hole creation in $Fe(CO)_5$ apparently enhances σ-bonding in the Fe–CO bonds (electron-density increase between Fe and C, Fig. 10) and polarizes the ligands (electron-density increase at C and decrease at O, Fig. 10). These changes also occur in $Fe(CO)_4$ and $Fe(CO)_3$ in the intact Fe–CO bonds, and the chemical shift upon deligation has to be explained by additional electron-density changes that are visible locally at Fe (within 1-2 Å). Indeed, in $Fe(CO)_4$, the core hole (spherical electron-density decrease around Fe in Fig. 10) is additionally screened by a strong electron-density increase located along the broken bond (site 1 in Fig. 10), thus indicating a correlation between core-hole screening or chemical shift and coordination. This enhanced screening explains the Fe 3p shift to lower binding energies in $Fe(CO)_4$. Inspection of the shapes of all

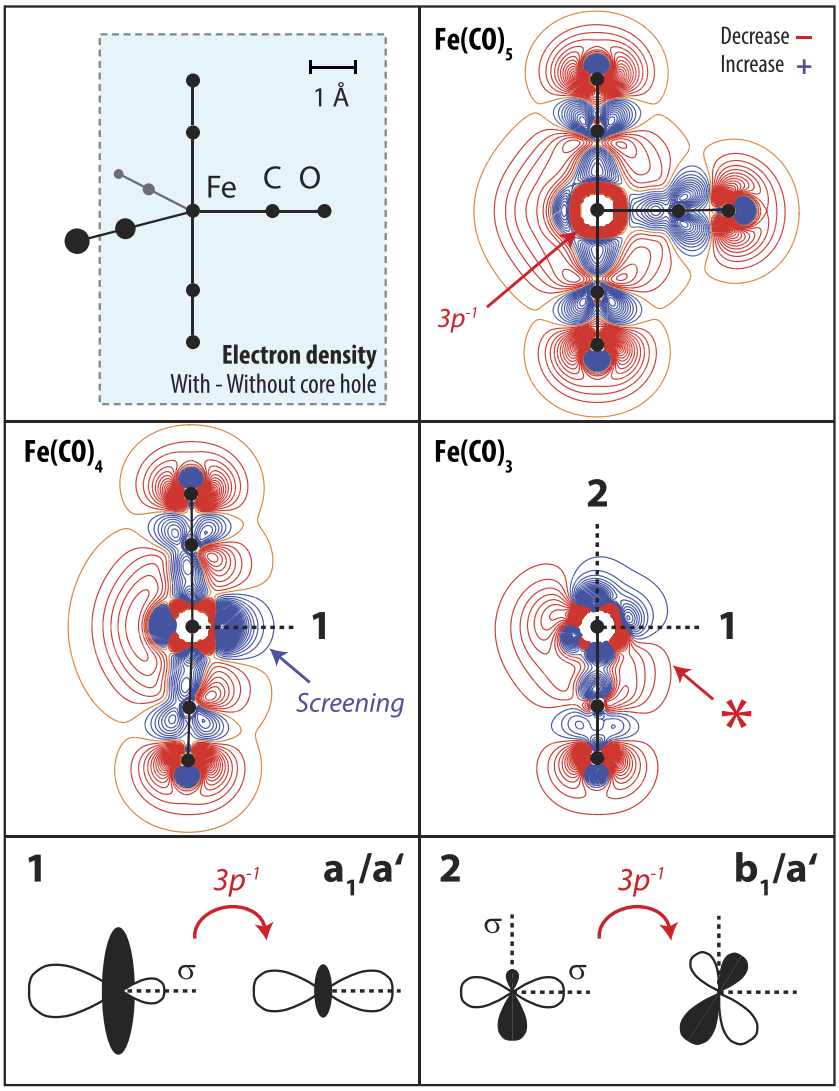

FIG. 10. Calculated electron-density changes in $Fe(CO)_5$, $Fe(CO)_4$, and $Fe(CO)_3$ upon 3p core-hole creation visualizing the changing capability for screening the core hole with changing coordination [electron-density differences plotted as contour lines from subtracting electron densities without the core hole from electron densities with the core hole in the respective species, plotted in the vertical plane indicated in the top left panel, decreasing/increasing electron density in red/blue; contour line spacings are 0.0005 electrons for $Fe(CO)_5$, 0.0006 electrons for $Fe(CO)_4$, and 0.001 electrons for $Fe(CO)_3$]. Positions where CO was removed are marked with **1** (equatorial CO) and **2** (axial CO). Bottom panels illustrate calculated changes of shapes of the a_1/a' and b_1/a' orbitals upon 3p core-hole creation for removal of an equatorial (**1**) and an axial CO (**2**) (orbital symmetries a_1/a' and b_1/a' for $Fe(CO)_4/Fe(CO)_3$ geometries). Fe 3p photoelectron spectra corresponding to these electron-density differences are plotted in Fig. 9.

calculated orbitals shows that this increase is due to the localization of the HOMO a_1 orbital along the direction of the disrupted bond upon 3p core-hole creation (orbital sketch for site 1 in Fig. 10, the shapes of all other orbitals remain unchanged). Apparently, deligation gives the occupied orbital that is oriented along the dissociated bond the freedom to reshape and thereby charge is localized accordingly. As a first indication of a general phenomenon, we find that this screening effect is also present in $Fe(CO)_3$ at the site where the second ligand was taken away (site 2 in Fig. 10). Again, the occupied orbital that is oriented along the dissociated bond (for site 2, this is the b_1/a' orbital sketched in Fig. 10) localizes in the direction of the disrupted bond and thereby electron density increases in this direction upon core-hole creation. In $Fe(CO)_3$, however, we find an additional core-hole effect at site 1 when taking away the ligand at site 2 that seems to compensate the screening thus balancing the chemical shift. This is revealed when inspecting the orbital populations of occupied and unoccupied orbitals upon Fe 3p core hole creation; see Table I. In addition to orbital reshaping, Fe 3p core-hole creation in $Fe(CO)_3$ entails population transfer from occupied to unoccupied molecular orbitals and mostly from HOMO $e'/a_1/a'$ (−0.14) to LUMO $a_1'/a_1/a'$ (+0.35). In $Fe(CO)_4$ and $Fe(CO)_5$, by contrast, all occupied orbitals equally loose population, while the LUMO gains in population and the orbital population changes are smaller than in $Fe(CO)_3$. For $Fe(CO)_3$, this transfer of orbital population from the localized HOMO $e'/a_1/a'$ to the

TABLE I. Multiconfigurational self-consistent-field (MCSCF) calculations of natural orbital populations upon 3p core-hole creation for $Fe(CO)_5$, $Fe(CO)_4$, and $Fe(CO)_3$. Population changes (orbital population with minus without the 3p core hole) are given in fractions of one electron for four occupied d_π and one unoccupied $d_\sigma*$ orbital [orbitals listed in the order of increasing orbital energy from left to right, orbital symmetries given for $[Fe(CO)_5/Fe(CO)_4]/Fe(CO)_3$ geometries, the column denoted $d_\pi*$ gives the summed changes of four unoccupied orbitals, one occupied d_π orbital with nearly constant population is not shown, a total of ten orbitals was used in the active space].

	d_π				$d_\sigma*$	$d_\pi*$
Orbital	$e''/a_2/a''$	$e''/b_1/a'$	$e'/b_2/a''$	$e'/a_1/a'$	$a_1'/a_1/a'$	4 MOs
$Fe(CO)_5$	−0.02	−0.02	−0.04	−0.04	+0.11	+0.04
$Fe(CO)_4$	−0.02	−0.04	−0.04	−0.06	+0.18	−0.03
$Fe(CO)_3$	−0.05	−0.05	−0.06	−0.14	+0.35	−0.06

comparably delocalized LUMO $a_1'/a_1/a'$ (the LUMO considerably extends out to the CO ligands; see Refs. 1 and 26) effectively corresponds to, upon core-hole creation, charge delocalization from Fe into the plane of the molecule. This results in electron-density decrease between equatorial ligands, as is visible in the electron-density differences at the corresponding site 1 in $Fe(CO)_3$ (marked with * in Fig. 10). Therefore both depopulation of the HOMO $e'/a_1/a'$ (localized along site 1) and the electron-density decrease between equatorial ligands compensate the electron-density increase at site 1 by orbital reshaping, thus limiting the chemical shift in $Fe(CO)_3$ to the effect at site 2. This, we believe, explains the lack in the change of the Fe 3p binding energy when going from $Fe(CO)_4$ to $Fe(CO)_3$.

The way final-state core-hole effects determine Fe 3p core-level binding energies in $Fe(CO)_5$, $Fe(CO)_4$, and $Fe(CO)_3$ is summarized with the total-energy diagram shown in Fig. 11. Dissociation of $Fe(CO)_5$ to $Fe(CO)_4$ and $Fe(CO)_3$ corresponds to increasing the ground-state energy of the system by 2.1 and 4.1 eV, respectively. These (neutral) ground states are the initial states for the photoemission process, and the Fe 3p binding energy corresponds to the energy difference between this ground state and the (ionic) final states (for simplicity, in Fig. 11, we consider the average of the three final states only). With $Fe(CO)_5$ as a reference and without the changes in the ability to screen the Fe 3p core hole in $Fe(CO)_4$ and $Fe(CO)_3$ compared to $Fe(CO)_5$, the Fe 3p binding energies would remain unchanged compared to $Fe(CO)_5$ (shift of 0 eV in Fig. 11). The additional capabilities for screening the core hole in the core-hole states of $Fe(CO)_4$ or $Fe(CO)_3$ by orbital reshaping as depicted in Fig. 10, however, reduce the Fe 3p binding energy E_B of $Fe(CO)_5$. This additional screening stabilizes the Fe 3p core-hole states and causes the observed shifts to lower binding energies from $Fe(CO)_5$ to $Fe(CO)_4$ or $Fe(CO)_3$ ($E_B^{expt.}-E_B < 0$ in the experiment or $E^{theo.}-E_B < 0$ in theory; note that the accuracy with which the dissociation energies are calculated does not affect the accuracy of the calculated binding-energy shifts $E_B{}^{theo.}-E_B$). The binding energy does not change from $Fe(CO)_4$ to $Fe(CO)_3$ because $Fe(CO)_3$ does not exhibit any additional screening capabilities compared to $Fe(CO)_4$. Further studies will show how general this concept of correlating metal core-level binding-energy shifts with coordination in metal complexes is. A preliminary comparison of Fe–CN and Fe–CO bonds at the geometries studied here indicates that the calculated shift may be independent of the nature of the ligand. This points at a general concept for probing metal coordination in complexes similar to the established "excited-atom model"[86] explaining ligand core-level binding-energy shifts upon coordination to metal atoms in complexes or on surfaces.[80,81]

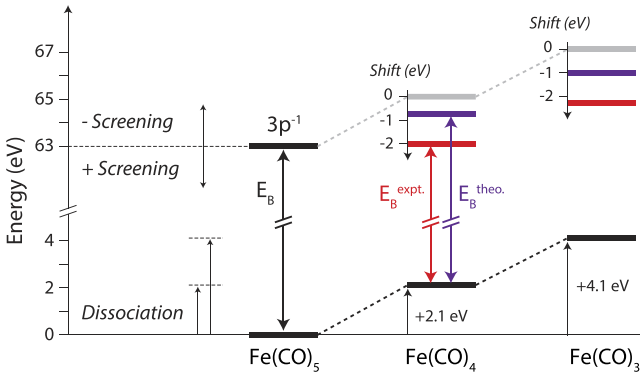

FIG. 11. Total-energy diagram drawn to scale with energies of neutral initial ground states and ionic final core-excited $3p^{-1}$ states of $Fe(CO)_5$, $Fe(CO)_4$, and $Fe(CO)_3$ from the experiment ($E_B{}^{expt.}$) and multiconfigurational self-consistent-field (MCSCF) calculations [$E_B{}^{theo.}$ are mean values averaged for the different final ionic states in each system, the initial ground-state energy of $Fe(CO)_5$ was set to zero, the calculated dissociation energies of +2.1 and +4.1 eV define the initial-state energies of $Fe(CO)_4$ and $Fe(CO)_3$].

SUMMARY AND CONCLUSIONS

Coordination and charge density or bonding of the short-lived reaction intermediates $Fe(CO)_4$ and $Fe(CO)_3$ in $Fe(CO)_5$ photodissociation are revealed with optical pump and x-ray probe photoelectron spectroscopy at an x-ray free-electron laser in combination with *ab initio* quantum-chemical calculations. We show how time-resolved valence photoelectron spectroscopy reflects changes in Fe–CO bonding and how this validates fundamental concepts for changes in frontier-orbital interactions in the dissociation of Fe–CO bonds. With time-resolved core-level photoelectron spectroscopy, we selectively probe and follow in time the evolution of different classes of chemically different environments of Fe and CO by measuring their transiently evolving chemical shifts. Multiconfigurational self-consistent field calculations are used to explain the Fe 3p core-level binding energy shifts upon Fe–CO dissociation with core-hole induced charge localization effects which enhance the capability to screen the core hole. The Fe 3p core-level binding energy shifts to lower energies from $Fe(CO)_5$ to $Fe(CO)_4$ and this is shown to be due to a stabilization of the core hole in $Fe(CO)_4$ due to enhanced screening by localized charge at the Fe core-hole site. For $Fe(CO)_3$, we also find this increased charge localization at the Fe core-hole site and we trace its origin back to a reshaped occupied orbitals along the broken Fe-CO bond directions. In $Fe(CO)_3$, additional changes in orbital populations with charge being transferred from the Fe site out to the ligands compensate this enhanced core hole screening thereby resulting in a constant binding energy from $Fe(CO)_4$ to $Fe(CO)_3$. This correlation of core-level binding energy, coordination and valence orbital shapes, and populations may represent the first step to establish a new way of probing coordination in 3d transition-metal complexes. In a more general sense, our results benchmark time-resolved optical pump and x-ray probe photoelectron spectroscopy for extracting charge-density dynamics in organometallic photoreactions. They further extend the demonstrated capabilities of steady-state electron spectroscopy for chemical analysis (ESCA) and of time-resolved photoelectron spectroscopy with optical probe pulses, thus complementing other time-resolved experimental techniques for the investigation of photochemical reactions.

ACKNOWLEDGMENTS

We thank the FLASH team for their excellent support during the beamtime. We are grateful to the machine operators,

the run coordinators, and we cordially thank Harald Redlin for the support in setting up the optical pump laser. This work was supported by the Helmholtz Virtual Institute "Dynamic Pathways in Multidimensional Landscapes" and the Volkswagen Stiftung (M.B.). M.O. acknowledges financial support from the Swedish Research Council (V.R.). I.J. acknowledges support by the Lennander Foundation. M.M. acknowledges support by the excellence cluster "The Hamburg Center for Ultrafast Imaging—Structure, Dynamics, and Control of Matter at the Atomic Scale" of the Deutsche Forschungsgemeinschaft (CUI, No. DFG-EXC1074). Support was given by the German Federal Ministry of Education and Research through the priority programme FLASH: "Matter in the light of ultrashort and extremely intense X-ray pulses" and Contract No. 05K10PK2. P.W. We thank Kelly Gaffney for important discussions.

[1] A. Albright, J. K. Burdett, and M.-H. Whangbo, *Orbital Interactions in Chemistry* (John Wiley & Sons, Inc., 2013).
[2] E. Koerner von Gustorf and F.-W. Grevels, "Photochemistry of metal carbonyls, metallocenes, and olefin complexes," Fortsch. Chem. Forsch. **13**, 366 (1969).
[3] N. Leadbeater, "Enlightening organometallic chemistry: The photochemistry of $Fe(CO)_5$ and the reaction chemistry of unsaturated iron carbonyl fragments," Coord. Chem. Rev. **188**, 35 (1999).
[4] M. Wrighton, "Photochemistry of metal carbonyls," Chem. Rev. **74**, 401 (1974).
[5] M. Poliakoff and E. Weitz, "Shedding light on organometallic reactions: The characterization of $Fe(CO)_4$, a prototypical reaction intermediate," Acc. Chem. Res. **20**, 408 (1987).
[6] L. Banares, T. Baumert, M. Bergt, B. Kiefer, and G. Gerber, "The ultrafast photodissociation of $FeCO_5$ in the gas phase," J. Chem. Phys. **108**, 5799 (1998).
[7] A. J. Ouderkirk, P. Werner, N. L. Schultz, and E. Weitz, "Observation of coordinatively unsaturated intermediates following the pulsed UV photolysis of $Fe(CO)_5$," J. Am. Chem. Soc. **105**, 3354 (1983).
[8] L. Banares, T. Baumert, M. Bergt, B. Kiefer, and G. Gerber, "Femtosecond photodissociation dynamics of $Fe(CO)_5$ in the gas phase," Chem. Phys. Lett. **267**, 141 (1997).
[9] M. Poliakoff and J. J. Turner, "Structure and reactions of matrix-isolated tetracarbonyliron(0)," J. Chem. Soc., Dalton Trans. **1974**, 2276.
[10] L. A. Barnes, M. Rosi, and C. W. Bauschlicher, Jr., "An *ab initio* study of $Fe(CO)_n$, $n = 1$,5, and $Cr(CO)_6$," J. Chem. Phys. **94**, 2031 (1991).
[11] C. Daniel, M. Benard, A. Dedieu, R. Wiest, and A. Veillard, "Theoretical aspects of the photochemistry of organometallics. III. Potential energy curves for the photodissociation of pentacarbonyliron ($Fe(CO)_5$)," J. Phys. Chem. C **88**, 4805 (1984).
[12] J. N. Harvey and M. Aschi, "Modelling spin-forbidden reactions: recombination of carbon monoxide with iron tetracarbonyl," Faraday Discuss. **124**, 129 (2003).
[13] A. A. Trushin, W. Fuss, K. L. Kompa, and W. E. Schmid, "Femtosecond dynamics of $Fe(CO)_5$ photodissociation at 267 nm studied by transient ionization," J. Phys. Chem. A **104**, 1997 (2000).
[14] M. Poliakoff and J. J. Turner, "The structure of $[Fe(CO)_4]$—An important new chapter in a long-running story," Angew. Chem., Int. Ed. **40**, 2809 (2001).
[15] H. Ihee, J. Cao, and A. H. Zewail, "Ultrafast electron diffraction of transient $[Fe(CO)_4]$: Determination of molecular structure and reaction pathway," Angew. Chem., Int. Ed. **40**, 1532 (2001).
[16] P. Wernet *et al.*, "Communication: Direct evidence for sequential dissociation of gas-phase $Fe(CO)_5$ via a singlet pathway upon excitation at 266 nm," J. Chem. Phys. **146**, 211103 (2017).
[17] H. Dachraoui *et al.*, "Photoinduced reconfiguration cycle in a molecular adsorbate layer studied by femtosecond inner-shell photoelectron spectroscopy," Phys. Rev. Lett. **106**, 107401 (2011).
[18] O. Geßner *et al.*, "Femtosecond multidimensional imaging of a molecular dissociation," Science **311**, 219 (2006).
[19] B. K. McFarland *et al.*, "Ultrafast X-ray Auger probing of photoexcited molecular dynamics," Nat. Commun. **5**, 4235 (2014).
[20] D. Strasser, F. Goulay, and S. R. Leone, "Transient photoelectron spectroscopy of the dissociative $Br_2(^1\Pi_u)$ state," J. Chem. Phys. **127**, 184305 (2007).
[21] P. Wernet, M. Odelius, K. Godehusen, J. Gaudin, O. Schwarzkopf, and W. Eberhardt, "Real-time evolution of the valence electronic structure in a dissociating molecule," Phys. Rev. Lett. **103**, 013001 (2009).
[22] R. Iikubo, T. Fujiwara, T. Sekikawa, Y. Harabuchi, S. Satoh, T. Taketsugu, and Y. Kayanuma, "Time-resolved photoelectron spectroscopy of dissociating 1,2-butadiene molecules by high harmonic pulses," J. Phys. Chem. Lett. **6**, 2463 (2015).
[23] J. Nishitani, C. W. West, C. Higashimura, and T. Suzuki, "Time-resolved photoelectron spectroscopy of polyatomic molecules using 42-nm vacuum ultraviolet laser based on high harmonics generation," Chem. Phys. Lett. **684**, 397 (2017).
[24] O. Gessner and M. Guhr, "Monitoring ultrafast chemical dynamics by time-domain x-ray photo- and auger-electron spectroscopy," Acc. Chem. Res. **49**, 138 (2016).
[25] G. Frenking and N. Fröhlich, "The nature of the bonding in tansition-metal compounds," Chem. Rev. **100**, 717 (2000).
[26] U. Radius, F. M. Bickelhaupt, A. W. Ehlers, N. Goldberg, and R. Hoffmann, "Is CO a special ligand in organometallic Chemistry? Theoretical investigation of AB, $Fe(CO)_4AB$, and $Fe(AB)_5$ (AB = N_2, CO, BF, SiO)," Inorg. Chem. **37**, 1080 (1998).
[27] K. Kunnus *et al.*, "Identification of the dominant photochemical pathways and mechanistic insights to the ultrafast ligand exchange of $Fe(CO)_5$ to $Fe(CO)_4EtOH$," Struct. Dyn. **3**, 043204 (2016).
[28] P. Wernet *et al.*, "Orbital-specific mapping of the ligand exchange dynamics of $Fe(CO)_5$ in solution," Nature **520**, 78 (2015).
[29] J. Ullrich, A. Rudenko, and R. Moshammer, "Free-electron lasers: New avenues in molecular physics and photochemistry," Annu. Rev. Phys. Chem. **63**, 635 (2012).
[30] R. Boll *et al.*, "Charge transfer in dissociating iodomethane and fluoromethane molecules ionized by intense femtosecond X-ray pulses," Struct. Dyn. **3**, 043207 (2016).
[31] B. Erk *et al.*, "Imaging charge transfer in iodomethane upon x-ray photoabsorption," Science **345**, 288 (2014).
[32] A. Rudenko and D. Rolles, "Time-resolved studies with FELs," J. Electron Spectrosc. Relat. Phenom. **204**, 228 (2015).
[33] B. Ahr, M. Chollet, B. Adams, E. M. Lunny, C. M. Laperle, and C. Rose-Petruck, "Picosecond X-ray absorption measurements of the ligand substitution dynamics of $Fe(CO)_5$ in ethanol," Phys. Chem. Chem. Phys. **13**, 5590 (2011).
[34] A. R. Attar, A. Bhattacherjee, and S. R. Leone, "Direct observation of the transition-state region in the photodissociation of CH_3I by femtosecond extreme ultraviolet transient absorption spectroscopy," J. Phys. Chem. Lett. **6**, 5072 (2015).
[35] F. Lackner, A. S. Chatterley, C. D. Pemmaraju, K. D. Closser, D. Prendergast, D. M. Neumark, S. R. Leone, and O. Gessner, "Direct observation of ring-opening dynamics in strong-field ionized selenophene using femtosecond inner-shell absorption spectroscopy," J. Chem. Phys. **145**, 234313 (2016).
[36] Y. Pertot *et al.*, "Time-resolved x-ray absorption spectroscopy with a water window high-harmonic source," Science **355**, 264 (2017).
[37] A. A. Attar, A. Bhattacherjee, C. D. Pemmaraju, K. Schnorr, K. D. Closser, D. Predergast, and A. R. Leone, "Femtosecond x-ray spectroscopy of an electrocyclic ring-opening reaction," Science **356**, 54 (2017).
[38] M. P. Minitti *et al.*, "Imaging molecular motion: Femtosecond x-ray scattering of an electrocyclic chemical reaction," Phys. Rev. Lett. **114**, 255501 (2015).
[39] V. Kimberg, A. Lindblad, J. Söderström, O. Travnikova, C. Nicolas, Y. P. Sun, F. Gel'mukhanov, N. Kosugi, and C. Miron, "Single-molecule x-ray interferometry: Controlling coupled electron-nuclear quantum dynamics and imaging molecular potentials by ultrahigh-resolution resonant photoemission and *ab initio* calculations," Phys. Rev. X **3**, 011017 (2013).
[40] T. Marchenko *et al.*, "Electron dynamics in the core-excited CS_2 molecule revealed through resonant inelastic x-ray scattering spectroscopy," Phys. Rev. X **5**, 031021 (2015).
[41] K. Nagaya *et al.*, "Ultrafast dynamics of a nucleobase analogue illuminated by a short intense x-ray free electron laser pulse," Phys. Rev. X **6**, 021035 (2016).
[42] A. Trabattoni *et al.*, "Mapping the dissociative ionization dynamics of molecular nitrogen with attosecond time resolution," Phys. Rev. X **5**, 041053 (2015).

[43]A. Stolow, A. E. Bragg, and D. M. Neumark, "Femtosecond time-resolved photoelectron spectroscopy," Chem. Rev. **104**, 1719 (2004).
[44]M. Dell'Angela *et al.*, "Real-time observation of surface bond breaking with an x-ray laser," Science **339**, 1302 (2013).
[45]M. Eckstein, C. H. Yang, F. Frassetto, L. Poletto, G. Sansone, M. J. Vrakking, and O. Kornilov, "Direct imaging of transient fano resonances in N_2 using time-, energy-, and angular-resolved photoelectron spectroscopy," Phys. Rev. Lett. **116**, 163003 (2016).
[46]T. W. Kim *et al.*, "Combined probes of X-ray scattering and optical spectroscopy reveal how global conformational change is temporally and spatially linked to local structural perturbation in photoactive yellow protein," Phys. Chem. Chem. Phys. **18**, 8911 (2016).
[47]P. M. Kraus and H. J. Wörner, "Time-resolved high-harmonic spectroscopy of valence electron dynamics," Chem. Phys. **414**, 32 (2013).
[48]W. Li, X. Zhou, R. Lock, S. Patchkovskii, A. Stolow, H. Kapteyn, and M. M. Murnane, "Time-resolved dynamics in N_2O_4 probed using high harmonic generation," Science **322**, 1207 (2008).
[49]Y. Ogi *et al.*, "Ultraviolet photochemical reaction of $[Fe(III)(C_2O_4)_3]^{3-}$ in aqueous solutions studied by femtosecond time-resolved X-ray absorption spectroscopy using an X-ray free electron laser," Struct. Dyn. **2**, 034901 (2015).
[50]J. Vura-Weis, C.-M. Jiang, C. Liu, H. Gao, J. M. Lucas, F. M. F. de Groot, P. Yang, A. P. Alivisatos, and S. R. Leone, "Femtosecond $M_{2,3}$-edge spectroscopy of transition-metal oxides: Photoinduced oxidation state change in α-Fe_2O_3," J. Phys. Chem. Lett. **4**, 3667 (2013).
[51]W. Ackermann *et al.*, "Operation of a free-electron laser from the extreme ultraviolet to the water window," Nat. Photonics **1**, 336 (2007).
[52]K. Tiedtke *et al.*, "The soft x-ray free-electron laser FLASH at DESY: Beamlines, diagnostics and end-stations," New J. Phys. **11**, 023029 (2009).
[53]P. Radcliffe *et al.*, "An experiment for two-color photoionization using high intensity extreme-UV free electron and near-IR laser pulses," Nuclear Instrum. Methods Phys. Res., Sect. A **583**, 516 (2007).
[54]N. Gerasimova, S. Dziarzhytski, and J. Feldhaus, "The monochromator beamline at FLASH: Performance, capabiliti4es and upgrade plans," J. Mod. Opt. **58**, 1480 (2011).
[55]M. Martins, M. Wellhöfer, J. T. Hoeft, W. Wurth, J. Feldhaus, and R. Follath, "Monochromator beamline for FLASH," Rev. Sci. Instrum. **77**, 115108 (2006).
[56]M. Wellhöfer, M. Martins, W. Wurth, A. A. Sorokin, and M. Richter, "Performance of the monochromator beamline at FLASH," J. Opt. A: Pure Appl. Opt. **9**, 749 (2007).
[57]P. Radcliffe *et al.*, "Single-shot characterization of independent femtosecond extreme ultraviolet free electron and infrared laser pulses," Appl. Phys. Lett. **90**, 131108 (2007).
[58]H. Redlin, A. Al-Shemmary, A. Azima, N. Stojanovic, F. Tavella, I. Will, and S. Düsterer, "The FLASH pump–probe laser system: Setup, characterization and optical beamlines," Nuclear Instrum. Methods Phys. Res., Sect. A **635**, S88 (2011).
[59]K. Tiedtke *et al.*, "Gas detectors for x-ray lasers," J. Appl. Phys. **103**, 094511 (2008).
[60]S. Düsterer *et al.*, "Development of experimental techniques for the characterization of ultrashort photon pulses of extreme ultraviolet free-electron lasers," Phys. Rev. Spec. Top. - Accel. Beams **17**, 120702 (2014).
[61]F. Aquilante *et al.*, "MOLCAS 8: New capabilities for multiconfigurational quantum chemical calculations across the periodic table," J. Comput. Chem. **37**, 506 (2016).
[62]J. Finley, P. A. Malmqvist, B. O. Roos, and L. Serrano-Andrés, "The multi-state CASPT2 method," Chem. Phys. Lett. **288**, 299 (1998).
[63]B. O. Roos, R. Lindh, P. A. Malmqvist, V. Veryazov, and P.-O. Widmark, "Main group atoms and dimers studied with a new relativistic ANO basis set," J. Phys. Chem. A **108**, 2851 (2004).
[64]B. O. Roos, R. Lindh, P. A. Malmqvist, V. Veryazov, and P.-O. Widmark, "New relativistic ANO basis sets for transition metal atoms," J. Phys. Chem. A **109**, 6575 (2005).
[65]G. Grell, S. I. Bokarev, B. Winter, R. Seidel, E. F. Aziz, S. G. Aziz, and O. Kuhn, "Multi-reference approach to the calculation of photoelectron spectra including spin-orbit coupling," J. Chem. Phys. **143**, 074104 (2015).
[66]P. A. Malmqvist, A. Rendell, and B. O. Roos, "The restrlcted active space self-consistent-field method, implemented with a split graph unitary group approach," J. Phys. Chem. **94**, 5477 (1990).
[67]B. O. Roos, P. R. Taylor, and P. E. M. Siegbahn, "A complete active space SCF method (CASSCF) using a density matrix formulated super-CI approach," Chem. Phys. **48**, 157 (1980).
[68]M. Douglas and N. M. Kroll, "Quantum electrodynamical corrections to the fine structure of helium," Ann. Phys. **82**, 89 (1974).
[69]B. A. Hess, "Relativistic electronic-structure calculations employing a two component nopair formalism with external-field projection operators," Phys. Rev. A **33**, 3742 (1986).
[70]P. Å. Malmqvist, B. O. Roos, and B. Schimmelpfennig, "The restricted active space (RAS) state interaction approach with spin-orbit coupling," Chem. Phys. Lett. **357**, 230 (2002).
[71]M. Ohno and G. A. van Riessen, "Hole-lifetime width: A comparison between theory and experiment," J. Electron Spectrosc. Relat. Phenom. **128**, 1 (2003).
[72]R. Fukuda, M. Ehara, H. Nakatsuji, N. Kishimoto, and K. Ohno, "Valence ionized states of iron pentacarbonyl and η5-cyclopentadienyl cobalt dicarbonyl studied by symmetry-adapted cluster-configuration interaction calculation and collision-energy resolved Penning ionization electron spectroscopy," J. Chem. Phys. **132**, 084302 (2010).
[73]D. Guenzburger, E. M. B. Saitovitch, M. A. De Paoli, and H. Menala, "On the photofragmentation of $Fe(CO)_5$. II. Molecular orbital studies of $Fe(CO)_n$, $1 \geq n \geq 5$," J. Chem. Phys. **80**, 735 (1984).
[74]J. L. Hubbard and D. L. Lichtnberger, "The Jahn-Teller effect in the photoelectron spectrum of iron pentacarbonyl," J. Chem. Phys. **75**, 2560 (1981).
[75]J. Gladh, H. Oberg, J. Li, M. P. Ljungberg, A. Matsuda, H. Ogasawara, A. Nilsson, L. G. Pettersson, and H. Ostrom, "X-ray emission spectroscopy and density functional study of CO/Fe(100)," J. Chem. Phys. **136**, 034702 (2012).
[76]U. Gelius, "Binding energies and chemical shifts in ESCA," Phys. Scr. **9**, 133 (1974).
[77]K. Siegbahn *et al.*, *ESCA Applied to Free Molecules* (North-Holland Publ. Co., Amsterdam, 1996).
[78]B. Johansson and N. Mårtensson, "Core-level binding-energy shifts for the metallic elements," Phys. Rev. B **21**, 4427 (1980).
[79]H. J. Freund and E. W. Plummer, "Explanation of the satellite structure observed in the photoemission spectra of coordinated CO," Phys. Rev. B **23**, 4859 (1981).
[80]A. Nilsson, N. Martensson, S. Svensson, L. Karlsson, D. Nordfors, and U. Gelius, "High resolution x-ray photoelectron spectroscopy study of $Cr(CO)_6$ in the gas phase," J. Chem. Phys. **96**, 8770 (1992).
[81]E. W. Plummer, C. T. Chen, W. K. Ford, W. Eberhardt, R. P. Messmer, and H.-J. Freund, "A comparison of surface electron spectroscopies," Surf. Sci. **158**, 58 (1985).
[82]E. W. Plummer, W. R. Salaneck, and J. S. Miller, "Photoelectron spectra of transition-metal carbonyl complexes: Comparison with the spectra of adsorbed CO," Phys. Rev. B **18**, 1673 (1978).
[83]E. Sistrunk, J. Grilj, B. K. McFarland, J. Rohlen, A. Aguilar, and M. Guhr, "Resonant photoemission at the iron M-edge of $Fe(CO)_5$," J. Chem. Phys. **139**, 164318 (2013).
[84]F. A. Delesma, M. Van den Bossche, H. Gronbeck, P. Calaminici, A. M. Koster, and L. G. M. Pettersson, "A chemical view on x-ray photoelectron spectroscopy: The ESCA molecule and surface-to-bulk XPS shifts," Chemphyschem **19**, 169 (2018).
[85]N. Martensson and A. Nilsson, "On the origin of core-level binding energy shifts," J. Electron Spectrosc. Relat. Phenom. **75**, 209 (1995).
[86]N. D. Lang and A. R. Williams, "Core holes in chemisorbed atoms," Phys. Rev. B **16**, 2408 (1977).